The application of atomic force microscopy in mineral flotation - A critical review

Butt, H.-J.; Xing, Y.; Gui, X.; Cao, Y.; Babel, B.; Rudolph, M.; Weber, S.; Kappl, M.;

Originally published:

June 2018

Advances in Colloid and Interface Science 256(2018), 373-392

DOI: https://doi.org/10.1016/j.cis.2018.01.004

Perma-Link to Publication Repository of HZDR:

https://www.hzdr.de/publications/Publ-26035

The application of atomic force microscopy in mineral flotation - A critical review

Yaowen Xing[1,3], Xiahui Gui[2,3],Yijun Cao[2], Bent Babel[4], Martin Rudolph[4], Stefan Weber[3], Michael Kappl[3,*], Hans-Jürgen Butt[3,*]

1. School of Chemical Engineering and Technology, China University of Mining and Technology, Xuzhou 221116, China;

2. Chinese National Engineering Research Center of Coal Preparation and Purification, Xuzhou 221116, China;

3. Max Planck Institute for Polymer Research, Ackermannweg 10, 55128 Mainz, Germany;

4. Helmholtz-Zentrum Dresden-Rossendorf, Helmholtz Institute Freiberg for Resource Technology, Chemnitzer Str. 40, 09599 Freiberg, Germany.

*Corresponding author: butt@mpip-mainz.mpg.de (Butt H.); kappl@mpip-mainz.mpg.de (Kappl M.)

Abstract

During the past years, atomic force microscopy (AFM) has matured to an indispensable tool to characterize nanomaterials in colloid and interface science. For imaging, a sharp probe mounted near to the end of a cantilever scans over the sample surface providing a high resolution three-dimensional topographic image. In addition, the AFM tip can be used as a force sensor to detect local properties like adhesion, stiffness, charge etc. After the invention of the colloidal probe technique it has also become a major method to measure surface forces. In this review, we highlight the advances in the application of AFM in the field of mineral flotation, such as mineral morphology imaging, water at mineral surface, reagent adsorption, inter-particle force, and bubble-particle interaction. In the coming years, the complementary characterization of chemical composition such as using infrared spectroscopy during AFM topography imaging and the synchronous measurement of the force and distance involving deformable bubble as a force sensor will further assist the fundamental understanding of flotation mechanism.

***Keywords**: atomic force microscopy, mineral flotation, surface imaging, inter-particle force, bubble-particle interaction*

Contents

1. Introduction

Atomic force microscopy (AFM) belongs to the family of scanning probe microscopy. It was first developed by Binnig et al. [1] in 1986, for imaging the surface topography at nanometer resolution [2]. A sharp probe mounted near the end of a cantilever is raster scanned along the sample surface. The deflection of the cantilever is monitored by using an optical lever. Cantilever deflection is proportional to the force acting on the tip. Usually a feedback loop is used to keep the force between tip and sample constant by moving the sample up and down during scanning. In that case the height of the sample is plotted versus the lateral position to obtain a topographic image. Compared to electron microscopy, AFM has the advantages of imaging a surface both in air or liquid rather than in high vacuum condition, and providing a three-dimensional surface profile [3].

Soon after, it was used as a force sensor to measure forces, including surface forces, adhesion force, and hydrodynamic force, between different surfaces or molecules of interest, especially with the aid of the so called “colloid probe technique” [4-6]. In the colloid probe technique, a micrometer-size particle with well-defined geometry is attached to the end of the cantilever in order to replace the sharp tip. Usually the particle is spherical to facilitate the quantitative analysis. Thus, the interaction geometry between the probe and surface is greatly simplified. The force is obtained by multiplying the spring constant of the cantilever and the deflection. Currently, AFM has matured to an indispensable surface analytical tool to characterize nanomaterials in colloid and interface science[7].

Froth flotation, belonging to the family of heterocoagulation separation techniques, is based on the difference in surface hydrophobicity of dispersed particles. It has been widely used in mineral processing [8-11], fine coal upgrading [12-14], wastewater treatment [15, 16], oil

sands processing [17, 18], fly ash decarburization [19-21] and pulp-deinking [22, 23]. For mineral flotation, when the raw minerals are collected from the underground, crushing and grinding is required for liberating the valuable components from the interlocking particles. Then, these fine particles are mixed with water and conditioned with appropriate reagents (collectors, frothers, depressants and regulators). Air is finally introduced and hydrophobic particles are captured by the rising bubbles while hydrophilic particles remain in the pulp. The essential sub-processes in a flotation cell are: wetting, reagents adsorption on minerals, inter-particle force, and bubble-particle interaction. Each step plays a critical role in final flotation recovery. A comprehensive understanding of these sub-processes is of great fundamental and practical importance to design high-efficiency flotation process.

Up to now, a number of studies have been carried out to investigate these sub-processes. Contact angle measurement is the most commonly used method in the study of mineral-water wetting [24]. Spectroscopic techniques such as infrared spectroscopy, X-ray photoelectron spectroscopy and sum-frequency generation spectroscopy (V-SFG) are usually applied to better understand reagent adsorption on mineral surface and water structure at mineral-water interface [25-29]. Zeta potentials are measured to characterize the charge on particles which is essential to predict inter-particle electrostatic interaction. Theory and computational fluid dynamics are reported to study hydrodynamic inter-particle or bubble-particle interaction [30-36]. In addition, AFM is also a powerful tool for flotation engineering since it has the ability to investigate all sub-processes in flotation at the nanoscale.

The aim of this review is to demonstrate the versatility, flexibility, and future potential of AFM in order to shed new light on the flotation mechanisms. We highlight the current state of the art in the application of AFM in the field of mineral flotation, such as mineral morphology

imaging, water at mineral surface, reagent adsorption, inter-particle force, and bubble-particle interaction. Limitations and future perspectives are also discussed. This review is presented in a way that is accessible and valuable to flotation researchers with basic knowledge background regarding AFM.

2. Imaging of minerals

In most cases, AFM was used to image pure mineral surfaces such as mica, galena, molybdenite and phyllosilicate which can be easily cleaved [37-42]. For example, Xie et al. [39] studied the effect of applied electrochemical potential, with regard to the Ag/AgCl/3.4 M KCl reference electrode, on the galena surface morphology. It was found that surface roughness increased significantly when the potential exceeded +0.3 V. This was due to the agglomeration of electrochemical oxidation products on the galena surface. Hampton et al. [42] studied the effect of applied potential on electrochemical oxidation of the galena surface at pH 4.5 (Fig. 1). Sulphur domains were observed and surface roughness increased when the electrochemical potential increased to +258 mV. The difference between the two reports is that Hampton et al. [42] concluded that the electrochemical oxidation of galena is a two-step process: First, sulphur is released into the solution and then the sulphur deposits on favourable sites; the sulphur domains are distributed heterogeneously (Fig. 1), while in Xie's report [39], the sulphur domains were more homogeneously distributed. The reason for this discrepancy may be due to the increased surface roughness of galena in Hampton's experiment. Surface heterogeneity led to a heterogeneous distribution of oxidation products.

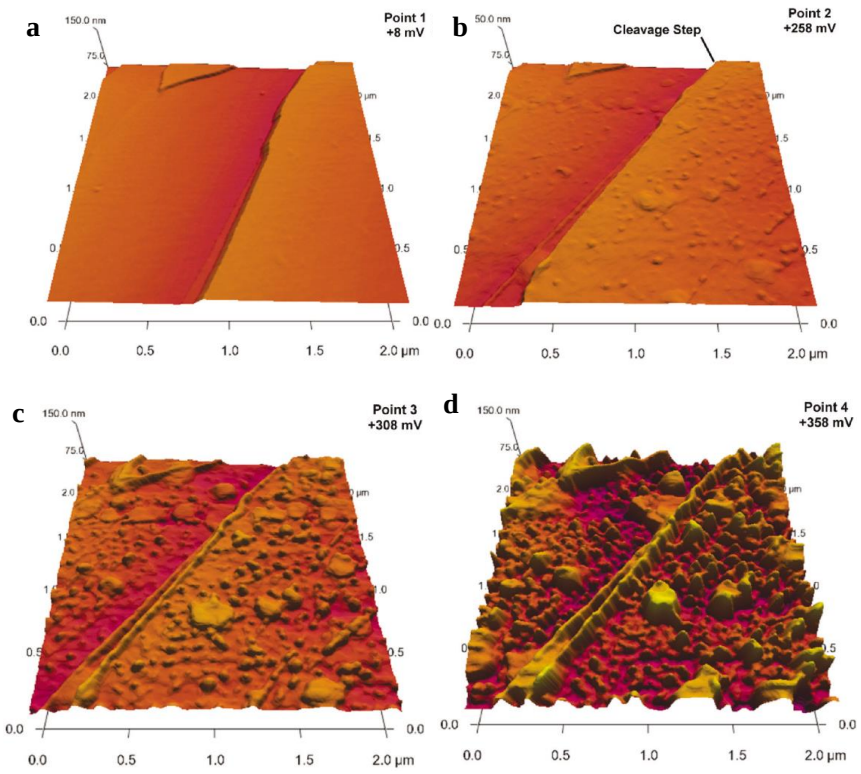

Fig. 1 Surface topographies of galena surfaces under different applied potentials: a, +8 mV; b, +258 mV; c, +308 mV; d, +358 mV. Adapted with permission from [42], Copyright 2011, American Chemical Society

Gupta et al. [41, 43] used AFM for imaging the silica and alumina faces of phyllosilicate (kaolinite). Negatively charged glass or mica and positively charged alumina were used as the substrates for kaolinite deposition. Due to the electrostatic double-layer attraction force, the positively charged alumina face of kaolinite particles attached to the glass or mica surface, thus exposing the silica faces. In contrast, the alumina face of kaolinite particles was exposed, when alumina was used as a substrate. It was found that tetrahedral oxygen atoms on the silica face formed a closed hexagonal ring-like network with a vacancy in the centre. On the other face, the hexagonal lattice ring of hydroxyls surrounded a hydroxyl.

For non-pure minerals which do not have a cleavage face, pre-treatment such as polishing is needed to lower the surface roughness so that it can be imaged by AFM. Bruening and Cohen

[44] applied AFM to identify the surface roughness variations before and after coal oxidation. Morga [45] used AFM to study the effect of heat treatment on the surface roughness of semifusinite and fusinite. Heating increased the surface roughness of both semifusinite and fusinite. AFM also has the ability to characterize the pore structure on coal surfaces [46]. Dun et al. [47] found that magmatic intrusions have a great impact on the pore structures of coal. The pore size of low-rank bituminous coal was much larger than high-rank anthracite. As a result, the small molecular weight alkanes (collectors) are easily lost in the pores due to the capillary effect [13]. Indeed, a higher concentration of collector is usually required for low-rank coal flotation than that of high-rank anthracite.

3. Water at mineral surface

3.1 Water structure near the interface

AFM is capable of imaging mineral surfaces in liquid. In flotation, both hydrophilic and hydrophobic particles are in contact with water. The interaction of the water molecules with the surface atoms of the solid has an influence on the structure of the interfacial water. The microscopic details of water structures at the solid-water interface are the key information to understand the flotation mechanisms. Currently, the interfacial water structure is attracting great interest from researchers in the colloid and flotation area, and numerous studies have focused on it. Water molecules close to a hydrophilic surface have a strong attractive interaction with surface atoms, e.g. via hydrogen bonds, increasing the surface free energy. This interaction also leads to a structuring of the interfacial water, where water molecules on average reside longer at positions with strong interaction than at positions with lower interaction force. Hydration layers typically consist of 3-5 molecular layers and can lead to an

increased viscosity at the interface compared to bulk water [48-55].

Hydration layers are dynamic structures: the molecules of the first hydration layer are typically completely exchanged within nanoseconds [56]. At the hydrophobic solid-liquid interfaces, in contrast, a water exclusion zone was observed using high-resolution X-ray reflectivity and neutron reflectivity [57-59].

To map hydration structures with the tip of AFM is challenging because the tip-sample forces inside the hydration layers can be of the same order as the thermal fluctuations in standard AFM cantilevers. In 2005, Fukuma et al. [60] demonstrated true atomic resolution imaging on a mica surface in aqueous buffer solution by using an AFM with very low detector noise. The low noise in the system was important because to obtain atomic scale resolution, the amplitude of the cantilever oscillation had to be on the order of the size of a water molecule, i.e. less than one nanometer. Using small amplitude force distance spectroscopy, they also observed oscillations in the tip-sample force which they ascribed to the layering of water molecules in the tip-sample gap. This layering is consistent with reports by Israelachvili and Pashley [61] and Zachariah et al. [62]. Israelachvili and Pashley [61] found that the short-range hydration force between two mica surfaces in water showed an oscillatory profile with a mean periodicity of the water molecule diameter indicating the existence of ordered water layers. In contrast, Zachariah et al. [62] suggested that the hydrated ion layering is responsible for the oscillatory hydration force. However, information on the potential lateral ordering of water molecules at the interface was still missing. Thus, a couple of years later Fukuma extended his high-resolution AFM to enable three dimensional mapping of the tip-sample force [63]. In this 3D scanning force microscopy (3D-SFM), the tip is scanned up and down like the needle of a sewing machine while the lateral position is slowly changed in a

scanning motion. In the first 3D-SFM investigation on a mica surface in aqueous buffer solution, a hexagonal pattern of force peaks with the same periodicity as the mica substrate was observed. Above this first hydration layer, a second and a third layer of force peaks were observed with a lateral shift. Later, similar hydration structures were observed on hydrophilic surfaces like calcite, fluorite, and dolomite [52, 64, 65]. Recently, several groups have investigated theoretically how the measured force field is connected to the overlap of hydration layers of tip and surface [56, 66, 67]. It was found that the force maxima correspond to the undisturbed positions of water molecules at the surface and that the presence of the tip has only a minor influence on the measured water structure. Further improvements in terms of the measurement technique could be achieved by using small cantilevers combining high resonance frequency and low spring constant [68] and by improving the three dimensional scanning method [69].

3.2 Surface nanobubbles characterization

On hydrophobic surfaces under some circumstance nanobubbles or air are formed and are stable for many hours. Nanobubbles at solid-water interface are an important subject since studies show that an enhanced flotation recovery can be obtained by using nanobubbles [70, 71]. Parker et al. [72] first suggested that the discontinuities in AFM force curves between two hydrophobic surfaces were due to the presence of nanobubbles. Experimentally, surface nanobubbles were firstly imaged by using AFM tapping mode by Ishida et al. [73] and Lou et al. [74]. Subsequently, force mapping mode AFM [75-77], peak-force tapping mode AFM [78-80], and peak-force quantitative nano-mechanics mode AFM [81] were all reported as being capable to image nanobubbles (Fig. 2). However, it is still unclear how much the AFM

tip affects the nanobubbles and whether or not nanobubbles are even created through gas nucleation during the imaging [77, 82]. In parallel, non-invasive techniques have confirmed the existence of nanobubbles such as infrared spectroscopy [83, 84], total internal reflection fluorescence microscopy [85], cryo-scanning electron microscopy [86, 87], quartz crystal microbalance [88], time-resolved fluorescence microscopy [89], scanning synchrotron based scanning transmission soft X-ray microscopy [90] and small angle X-ray scattering [91]. The height of nanobubbles has been reported in the range of 10-100 nm, while the length of the three-phase contact line is in general between 50 and 500 nm [92]. It is anticipated that nanobubbles should rapidly dissolve into surrounding water due to a high internal Laplace pressure. However, the lifetime of nanobubbles is surprisingly long observed experimentally [93]. The stability of nanobubbles has been a hot research topic and many questions are still left unanswered after years of study. However, it is out of the scope of this paper to review the stability theory of nanobubbles ; an excellent recent review is [94].

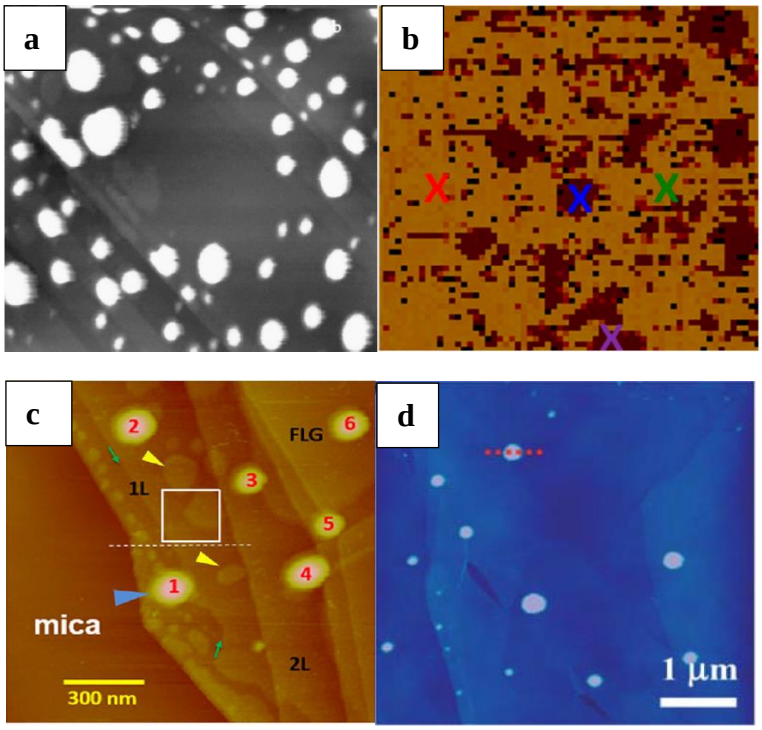

Fig. 2 Nanobubbles pictures imaged using different AFM working modes: (a) tapping mode, Reprinted with permission from [74], Copyright 2000, American Vacuum Society; (b) force mapping mode, Reprinted with permission from [75], Copyright 2013, American Chemical Society; (c) Peak-force tapping mode, Reprinted with permission from [79], Copyright 2016, American Chemical Society; (d) Peak-force QNM mode. Reprinted with permission from [81], Copyright 2013, The Royal Society of Chemistry

Using AFM, the effects of production methods, substrate properties, salts, solution pH, dissolved gas, surfactants, and temperature on nanobubbles can be studied. Previous studies showed that degassing pre-treatment reduces nanobubble formation [95, 96]. The gas type was also found to have great impact on nanobubble nucleation [97]. Zhang et al. [76, 98] found that pH, salts, and sodium dodecyl sulfate has little effect on nanobubbles stability, thus refuting the stability mechanism of the contamination skin hypothesis. Xu et al. [99] observed that the formation of surface nanobubbles was temperature-dependent. Much more nanobubbles were observed at high temperature than that at low temperature due to the higher gas saturation and faster molecular diffusion.

4. Reagent adsorption on mineral surface

4.1 Structure of adsorbed reagent

The interaction between flotation reagents and mineral surfaces are of particular interest. In flotation practice, various kinds of flotation reagents, i.e., collectors, frothers, dispersants, and flocculants, are used to regulate interfacial properties and thus the interaction between bubble and particle or inter-particle. Here, AFM can help analyzing the adsorption conformation of surfactants or polymers on mineral surface [38, 100-105]. Chennakesavulu et al. [104]

visualized the conformation of oleate collector on a fluorite crystal surface. Both monolayer and bilayer structures were observed even at low oleate concentration of 10^{-7} M. Paiva et al. [105] studied the effect of calcium ions on the adsorption of potassium oleate onto apatite surfaces. They found that calcium ions play a critical role in potassium oleate adsorption, since the adsorption was completed by forming calcium dioleate agglomerates. Beaussart et al. [38] explored the effect of three kinds of dextrins, a regular wheat dextrin (TY), carboxymethyl (CM) dextrin, and hydroxypropyl (HP) dextrin, on molybdenite flotation. Topographies of adsorbed dextrins on molybdenite surface were imaged using AFM (Fig. 3). The surface coverages of the modified dextrins (CM and HP) were much higher than that of regular TY, leading to a lower contact angle and flotation recovery.

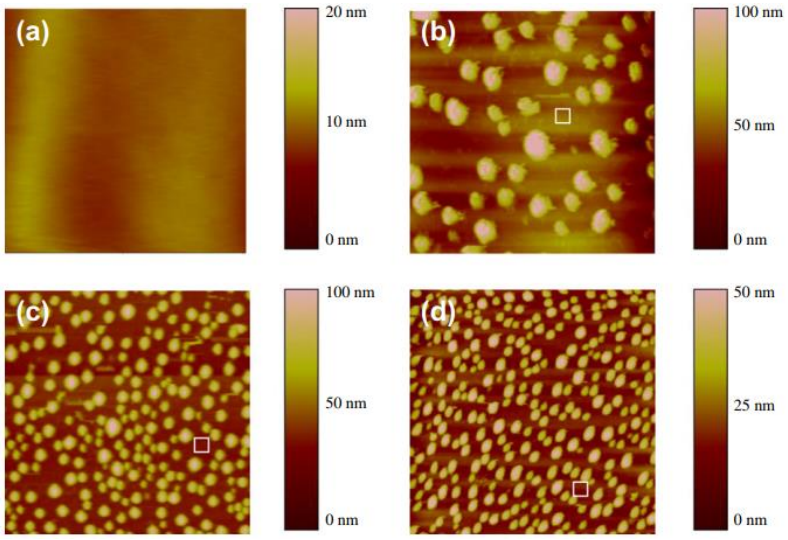

Fig. 3 Topographies of adsorbed dextrins on molybdenite surface: (a) bare molybdenite, (b) Dextrin TY, (c) CM Dextrin, (d) HP Dextrin. Reprinted with permission from [38], Copyright 2012, Elsevier

The effect of guar gum on molybdenite flotation was studied by Xie at al. [106]. The presence of polymer aggregates on molybdenite surfaces could be correlated with molybdenite flotation results. The flotation recovery of molybdenite decreased sharply from 69% to 11% and 3%

after guar gum adsorption at concentrations of 1 and 5 ppm. Mierczynska-Vasilev and Beattie [107] studied the adsorption of three kinds of substituted carboxymethyl cellulose on talc and chalcopyrite. The wettability depressions of three polymers on talc were always more effective than on chalcopyrite since more polymers adsorbed onto talc surface from AFM images. More specifically, low carboxymethyl cellulose coverage on both minerals was observed for a high substitution of the carboxymethyls.

4.2 Single molecule force spectroscopy

Polymers are often used as flocculants in ultra-fine particle flotation and filtration. Fine particles form large-size flocs under the bridging function of high-molecular-weight polymer. Theoretically, hydrogen bonding, the hydrophobic interaction, electrostatic attraction, and chemical bonding are the possible driving forces for flocculation. It was, however, difficult to measure the force between flocculant and mineral particle experimentally in earlier times. With the introduction of single molecule force spectroscopy (SMFS) it became possible to measure inter- and intramolecular interaction forces in polymer and supramolecular system with pN resolution using AFM [108-111]. Therefore, a polymer molecule bridge between AFM probe and substrate is formed. Then the bridge is stretched by slowly retracting the tip while measuring the force (Fig. 4).

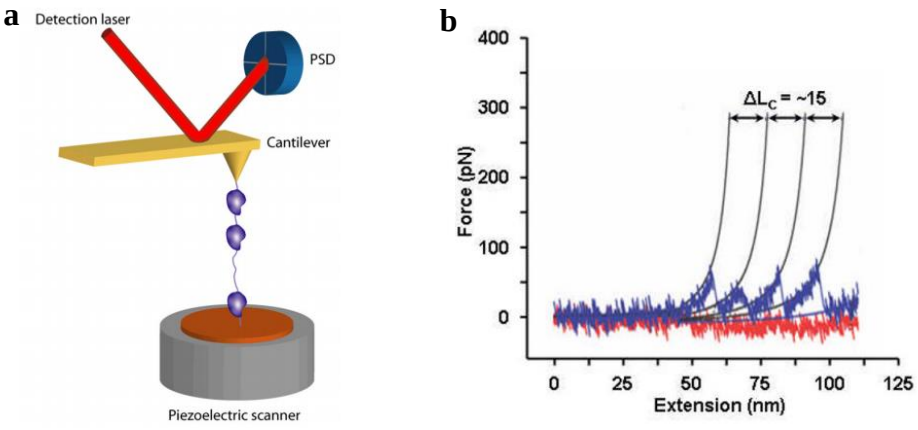

Fig. 4 (a) Schematic of SMFS; (b) Stretching force curves between a polyprotein molecule and a copper surface. ΔL_c is the contour length increment. Reprinted with permission from [109], Copyright 2012, Nature Publishing Group

Based on SMFS, Hugel et al. [112] studied the effect of polymer charge density and electrolyte concentration on the adhesion force between polyvinylamine chains and a negatively charged silica surface. The adhesion force decreased linearly with increasing electrolyte concentration and decreasing charge density. Long et al. [113] measured the adhesion force between a partially hydrolyzed polyacrylamide (HPAM) molecule and different kinds of surfaces (silica, mica, and bitumen). More specifically, in deionized water, the adhesion forces were reported to be 40, 200, and 80 pN on silica, mica, and bitumen surfaces, respectively (Fig. 5). When the process water from oil sand processing plant was used, the forces changed to 50, 100, and 40 pN, respectively. The adsorption strength between HPAM and mica was much higher than that on the bitumen surface. This indicated that a selective flocculation between clay particles, such as mica, can achieved when HPAM isadded to bitumen-clay mixture suspensions.

Sun et al. [114] carried out SMFS experiments between an $Al(OH)_3$-polyacrylamide (Al-PAM) and a silica surface. In this case, the $Al(OH)_3$ served as the core connecting a number of PAM chains. It was found that the adhesion force between $Al(OH)_3$ and silica was much higher than that between PAM chain and silica due to electrostatic attraction.

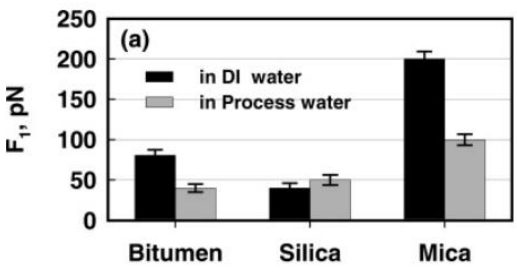

Fig. 5 Adhesion forces between HPAM and different kinds of surfaces in DI water and commercial plant process water. Reprinted with permission from [113], Copyright 2006, American Chemical Society.

Pensini et al. [115] directly coated carboxymethyl cellulose polymer on a fresh mica surface and a silica/borosilicate/iron oxide particle was attached to a tip-less cantilever. They recorded retraction forces between particles and CMC coated mica. Different rupture events could be identified from the shape of the force curves (Fig. 6). Compared to SMFS experiments, the bridge between the colloidal probe and mica surface is no longer formed by a single molecule. Instead a number of molecules interact due to the large contact area. It was found that the adhesion force between iron oxide and carboxymethyl cellulose coated mica in Milli-Q water was always higher than that between silica/borosilicate. Solution pH and ions were found to have great impact on the adhesion force.

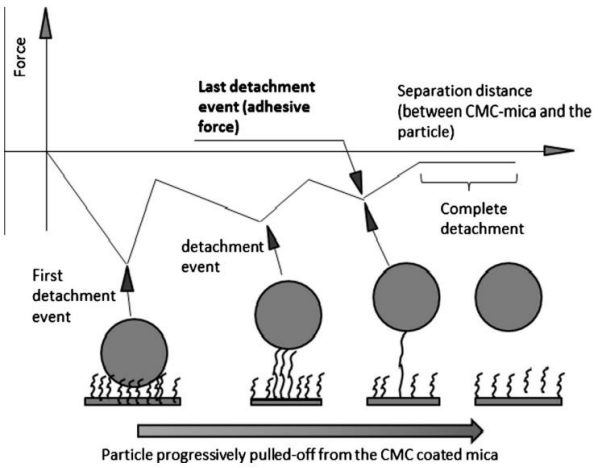

Fig. 6 Schematics of different rupture events during particle pull-off from carboxymethyl cellulose coated mica. Each minimum indicates a detachment event occurs. The last minimum is the adhesion force between one polymer molecule and colloid particle. Reprinted with permission from [115], Copyright 2013, Elsevier

High molecular-weight flocculants can be attached to the tip and their interaction with a mineral surface is relatively easy to measure. It is, however, difficult to directly measure the force between a single surfactant molecule (collector) and a mineral surface. Therefore, some substitutes were used to model collector-mineral interaction. Fa et al. [116, 117] prepared a calcium dioleate micro-sphere to model the interaction between the oleate collector and calcite/fluorite. More specifically, strong long-range attractive forces in approach curves and adhesion forces in retraction force curves were observed between calcium dioleate and fluorite; the force between calcium dioleate and calcite was much weaker. Indeed, such studies indicate that, in the presence of calcium, calcium dioleate forms firstly in bulk solution and then adsorbs in the form of calcium dioleate [118]. Xing et al. [119] used solid-state paraffin and stearic acid to represent conventional hydrocarbon oil and fatty acid collector in fine coal flotation. The interactions between paraffin/stearic acid and fresh/oxidized coal particles were measured directly using atomic AFM colloidal probe technique. In this case, the paraffin substrate for AFM experiments was prepared using section-cutting while stearic acid substrate was prepared by the pellet method. More specifically, a significant jump-into contact between oxidized coal particles and stearic acid was observed due to the hydrogen bonding while a monotonous repulsive force between oxidized coal and paraffin. Consequently, a fatty acid collector is more suitable for oxidized coal flotation than hydrocarbon oil.

5. Quantification of inter-particle force

The quantification of inter-particle force in colloid science is one of the most important applications of AFM [6]. Early work mainly focused on studying surface forces and verifying

the correctness of the Derjaguin-Landau-Verwey-Overbeek (DLVO) theory. Ducker et al. [4] first used AFM to measure the force between a hydrophilic silica sphere and a silica plane in presence of sodium chloride. The measured force at long range could be well predicted by the classical DLVO theory. However, a repulsive force at short range was observed probably due to the strong hydration of the surfaces. As the DLVO theory treats the intervening medium as continuous, the individual properties of molecules involved are not taken into consideration. Therefore, it cannot describe the an additional hydrogen force that is required to remove the water molecules at the interface when the distance decreases to a few molecular diameters [61]. Butt [5] also measured the force between a silicon nitride tip, alumina, glass, and diamond particle and glass/mica surface in presence of different salt concentrations. A repulsive hydration force with 3 nm decay length between silicon nitride tip and mica was observed at a high salt concentration (>3 M).

Another kind of non-DLVO force is the hydrophobic force. A vast amount of hydrophobic force results can be found in the literature. The first direct evidence of the hydrophobic force between hydrophobic mica surfaces was provided by Pashley and Israelachvili using a Surface Force Apparatus [120, 121]. They found that the hydrophobic force is much stronger than the van der Waals attraction and a single exponential function gave the best fit to the experimental data. Rabinovich and Yoon [122] found the hydrophobic force between a hydrophobic glass sphere and silica plate, measured using AFM, could be described with both exponential and power laws. Up to date, the origin of the hydrophobic force remains unclear. Both sample preparation methods and experimental techniques have great impact on the result [123]. Nanobubble bridging is one of the most representative mechanisms [124]. Hampton and Nguyen [125, 126] used a capillary mathematical model to fit the force curves between a

1-octanol esterified silica sphere and a silica plane, which supports nanobubble bridge hypothesis. Another possible mechanism for the long-range hydrophobic force is the formation of cavities. Cavitation due to metastability of the intervening liquid during approach or separation was proposed by Christensen and Claesson [127]. However, detailed discussion about these origin mechanisms is beyond the scope of this review. Readers who are interested in this topic can refer to the excellent reviews by Christenson and Claesson [123] and Meyer et al. [128].

From the flotation engineering point of view, slime coating and selective flocculation are the main areas where AFM can be applied to measure inter-particle force. For example, micro-fine minerals, mainly clays (kaolinite, illite, and montmorillonite), have a detrimental effect on coal flotation because they can easily form physisorbed coatings on coal surface [129, 130]. Such slime coatings make coal particles become hydrophilic and prevent bubbles or collectors from adhering to coal particles, reducing flotation recovery and increasing ash content of the concentrate. Measuring the driving force responsible for the slime coating is of both academic and practical importance.

In many cases it may be difficult to apply the DLVO theory to quantitatively describe the AFM measurement results due to the irregular geometry and surface heterogeneity of practical minerals. Still, the force curves can be qualitatively compared with varying the concentration of salt or pH and may provide guidance for flotation engineering. Xing et al. [129, 130] studied the effect of calcium ions on coal flotation in the presence of kaolinite clay. The interaction force between coal and kaolinite was measured using AFM (Fig. 7). Interestingly, no jump-in behavior was observed in de-ionized water and the repulsive force corresponded to that in the case of no kaolinite coating. A sudden jump-in was found when

Ca^{2+} increased to 3 mmol/L. The repulsive electrostatic force was suppressed by excessive Ca^{2+} addition, and the attractive force began to dominate the kaolinite particle interaction. The effect of clay types, i.e., kaolinite and montmorillonite on fine coal flotation was further studied [131]. Only a short jump-into-contact was observed in de-ionized water for coal-montmorillonite, which is responsible for lower flotation recovery and worse selectivity for the coal-montmorillonite system compared with that of coal-kaolinite.

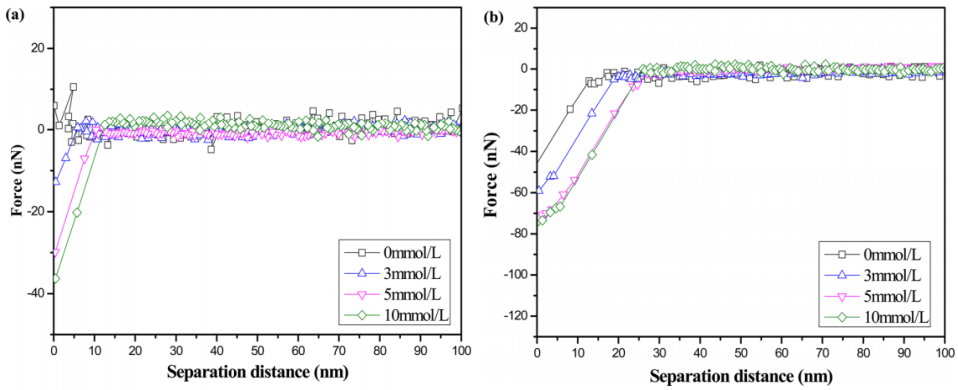

Fig.7 Force curves between coal substrate and a ~50-μm-diameter kaolinite particle in presence of different calcium concentrations: (a) approach curves; (b) retraction curves. Both attractive force and adhesion force increased with increasing calcium concentration. Reprinted with permission from [129], Copyright 2016, American Chemical Society.

Often it is more difficult to measure the inter-particle force in the presence of polymer due to experimental difficulties in controlling the polymer dose and the often irreversible adsorption [132, 133]. Nevertheless, Abraham et al. [134] measured the force between silica surfaces in the presence of copolymers of acrylamide and negatively charged acrylic acid with three different negative charge densities (i.e, 15%, 40%, and 70% acrylic acid fraction in copolymers). More specifically, at low charge density the force was repulsive in the range of experimental polymer concentrations (from 0.1 ppm to 50 ppm). Increasing the charge density

to 40 % or 70%, an attractive adhesion force was observed at a low polymer concentration due to polymer bridging. A purely repulsive force was observed again when the concentration increased to higher levels. Zhou et al. [135] also studied the effect of polymer charge density on the force between silica surfaces. Ofori et al. [136] examined the coal tailings flocculation performance using different types and concentrations of flocculants. The optimal flocculant concentration was the point corresponding to the maximum snap-off distance in AFM force curves.

Recently, a multi-particle colloidal probe technique (MPCPT) based on AFM-inverted optical microscope has been developed to measure inter-particle forces in situ with high precision in presence of polyelectrolyte [133, 137]. Silane reagents are used to hydrophobize a glass substrate and a tip-less AFM cantilever appropriately. A number of polystyrene latex particles are injected into the liquid cell to deposit the particles onto glass surface. Then, moving the cantilever on the upside of one particle and finishing attachment by hydrophobic force. Finally, force measurement is conducted between this colloid probe and another deposited particle. The main advantage of MPCPT, compared with that of traditional colloid particle probe only with one or two colloidal particles, is that the adsorption of polyelectrolyte on particles can be controlled precisely, due to the larger internal surface area in multi-particle suspension system.

Flotation is used for oil sands separation engineering. Oil sand separation has been studied, e.g. by Xu's and his team from Edmonton [138]. In oil sand processing, the first step is to liberate oil from the sand. The sand typically consists of carbonate rocks and silica. Then air bubbles are introduced to capture the heavy oil (bitumen) leaving sand particles in the pulp. It should be noted that clays also account for fifteen to thirty percent in raw oil sands [139].

Important sub-processes are: bitumen-sand liberation, bitumen-bubble interaction, and bitumen-fine particle interaction (clay coating). Here, we treat bitumen as the targeted particle similar to mineral flotation; therefore, we also briefly discuss the application of AFM in bitumen-sand liberation and clay coating in this section.

Liu et al. [140] coated a thin bitumen film on a flat silica wafer with a spin coater and then measured the force between bitumen and silica particle in 1 mM KCl solution. They found that both pH and calcium concentration play an important role in bitumen-silica interaction (Fig. 8). Not only did the repulsive barrier increase, but also the adhesion force decreased with increasing pH or decreasing calcium concentration. Temperature is also one of the most important parameters in oil sand processing. Increasing temperature reduces bitumen viscosity and thus decreases the adhesion force [141]. Alkaline solution with high temperature and low ion concentrations promotes bitumen liberation. Zhang et al. [142] further suggested a synergistic effect between surfactants (dodecyltrimethylammonium chloride and sodium dodecylbenzene sulfonate) and divalent cation ions (Ca^{2+} or Mg^{2+}) during bitumen–silica interaction. More specifically, in alkaline solution, sodium dodecylbenzene sulfonate does not adsorb on negatively charged silica and bitumen surfaces due to the strong repulsive double-layer force. However, this is not the case when divalent cation ions were added. Ca^{2+} or Mg^{2+} prefer adsorbing on silica and bitumen surface in the form of $CaOH^{+}$ and $MgOH^{+}$. Thus, these monohydroxyl species act as bridges between sodium dodecylbenzene sulfonate and the solid surface. Liu et al. [143] measured the force between bitumen and different kinds of clays (montmorillonite and kaolinite). Due to the irregularity of clay particles, force measurements were carried out several times and the final general trend was plotted. The adhesion force between bitumen and montmorillonite was always higher than that between

bitumen and kaolinite, especially in presence of Ca^{2+}. This is probably due to the large capacity of adsorption of calcium for montmorillonite.

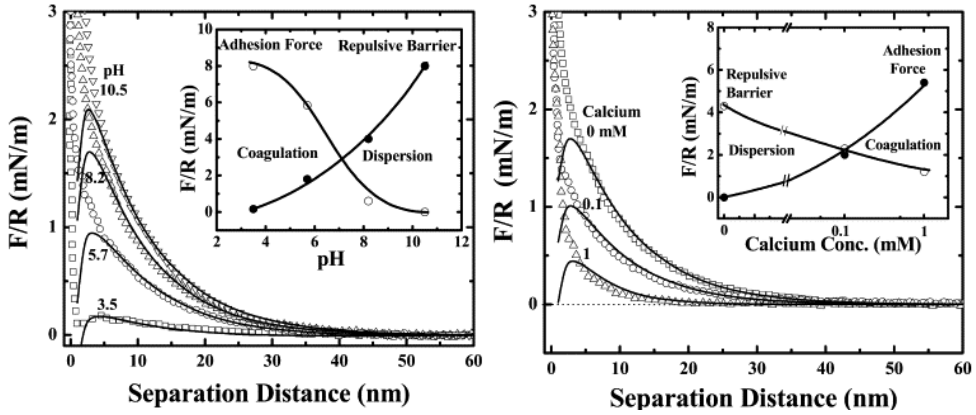

Fig. 8 The effect of pH and calcium concentration on the interaction between bitumen substrate and a ~5-10 μm silica particle in 1 mM KCl solution: (left) pH; (right) calcium concentration. The dashed and solid lines represent the experimental and theoretical fitting results, respectively. Reprinted with permission from [140], Copyright 2005, Elsevier

A related subject which should be briefly mentioned is bacteria-mineral interaction. A deep understanding of bacteria-mineral interaction force is critical to mineral bioleaching engineering. Measuring the force between bacterial and mineral by AFM, the main challenge is to anchor the bacteria onto the cantilever or flat substrate without affecting cell activity [144-146].

Lower et al. [147] introduced a new technique named biologically-active-force probe (BAFP) to measure the force between bacteria and different mineral surfaces (muscovite, goethite, and graphite). They used poly-D-lysine to functionalize glass beads; the negatively charged glass and cell-surfaces were bridged by positive charged poly-D-lysine in situ (Fig. 9). It was found that ions, mineral surface charge, and hydrophobicity significantly affected the interaction. Diao et al. [148] compared the adhesion forces between chalcopyrite and acidithiobacillus

thiooxidans/acidithiobacillus ferrooxidans under various pH conditions. The average adhesion force for acidithiobacillus ferrooxidans was always stronger than that of acidithiobacillus thiooxidans, especially under low pH conditions.

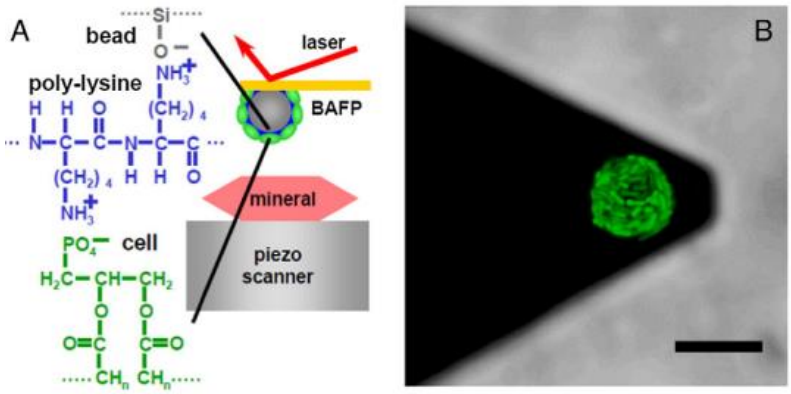

Fig. 9 (a) Schematic of BAFP, (b) Scanning laser confocal image of BAFP. The green particle is the cell coated glass. Scale bar is 10 μm. Reprinted with permission from [147], Copyright 2005, Elsevier

6. Bubble-particle interaction and thin liquid film drainage

Bubble-particle interaction is the critical step for flotation. It is well accepted that the hydrophobic force is responsible for successful bubble-particle attachment [149]. AFM offers a great opportunity to directly study bubble-particle interaction at a nanometer scale. Note that AFM force measurement between an air bubble and a solid particle is accompanied with the deformation of gas/liquid interface under both the hydrodynamic and surface forces. The dynamic coupling between force, bubble deformation and film drainage makes both theoretical analysis and experimental verification challenging [150, 151].

Ducker et al. [152] and Butt [153] first used AFM to measure the force between bubble and particle in 1994. A small hydrophilic or hydrophobic silica particle was attached to the end of AFM cantilever and then approached to the bubble surface at a low speed in pure water. The

observed attractive force between a hydrophilic particle and an air bubble in Ducker's experiment [152] probably due to contamination. When surfactant was added, the long range attractive force disappeared and a monotonous repulsive force emerged. In Butt's report [153], he found that a repulsive force acted between bubble and a hydrophilic glass. In contrast, a jump-into contact was observed when hydrophobic particles approached the bubble surface and a three-phase contact was formed.

The determination of zero distance is an essential step to convert AFM force-displacement curve to force-distance curve [154, 155]. Usually, the zero distance is deduced from constant compliance regime in a hard contact system. When bubble surface deformation is taken into consideration, it is difficult to find the hard contact point in bubble-particle force curves, thus the absolute separation distance is unknown. To solve this problem, the bubble was assumed to behave as a Hookean spring under external force. In this context, a number of bubble-particle force studies were conducted [156-161]. Ishida [158] studied the effect of surface hydrophobicity on bubble-particle interaction force. With increasing contact angle, the range of the attractive force increased whereas the wetting film rupture thickness did not changed significantly. Preuss and Butt [162, 163] studied the influence of dodecyltrimethylammonium bromide (DTAB) and sodium dodecyl sulfate (SDS) on bubble-silica interaction. It was found that hydrophobic force could be introduced between hydrophilic silica and bubble at moderate DTAB concentrations. However, hydrophobic force between hydrophobic silica and bubble was suppressed by adding SDS. Nguyen et al. [156, 157, 164] did a series of experiments on bubble-particle interaction using AFM. For a hydrophilic silica particle, the forces at different electrolyte concentrations could be well fitted by using classical DLVO theory. With increasing ion concentration, the electrostatic

force decreased due to the compression of the double electrostatic layer. The effect of approach velocity on the force between a hydrophilic glass sphere and bubble was also studied. The repulsive hydrodynamic force increased monotonically as the approach speed increased. When the particle became hydrophobic, a sudden jump-into contact due to the attractive hydrophobic force always observed at a low approach speed.

However, the simple assumption that the bubble surface behaves as a linear spring will not always be appropriate [165]. In recent years, significant progress has been achieved on both hydrodynamic drainage modelling and AFM-based experimental techniques. It has become possible to measure the force, bubble deformation, and liquid film drainage simultaneously [150].

Chan et al. [151, 166] derived a model called augmented Stokes-Reynolds-Young-Laplace model to predict the force and the evolution of the wetting film profile before the formation of three-phase contact line in dynamic AFM experiments. The augmented Stokes-Reynolds-Young-Laplace model under a no-slip boundary condition are [151]:

$$\frac{\partial h}{\partial t} = \frac{1}{12\mu r}\frac{\partial}{\partial r}\left(rh^3\frac{\partial p}{\partial r}\right) \quad (1)$$

$$p = \frac{2\gamma}{R} - \Pi - \frac{\gamma}{r}\frac{\partial}{\partial r}\left(r\frac{\partial h}{\partial r}\right) \quad (2)$$

where, h is the thickness of the intervening aqueous film, μ is the water viscosity, r is the radial distance from the center of the film, R is the bubble radius, p is the excess hydrodynamic pressure, γ is surface tension, Π is the disjoining pressure due to the van der Waals force, electrostatic force and hydrophobic force.

Eqs. (1) and (2) can be solved numerically in the region $0 \leq r \leq r_{max}$. r_{max} is selected as the value where the local separation h is so large that the contribution of disjoining pressure could be neglected. The Stokes-Reynolds-Young-Laplace model has the ability to capture the

essential physical characteristics in AFM force measurements and provides a basic understanding of bubble-particle interaction force and film drainage dynamics.

Shi et al. [167] measured the force between an air bubble and mica hydrophobized with octadecyltrichlorosilane (OTS) with different hydrophobicity in 500 mM NaCl solution. AFM force curves were fitted by using the Stokes-Reynolds-Young-Laplace model. A jump-into contact at 7.5 nm was experimentally observed for a partially hydrophobized mica with 45° water contact angle. The model reproduced the force results assuming a hydrophobic force with a decay length of 0.8 nm. Increasing the contact angle to 85°, both the critical film rupture thickness and hydrophobic force decay length increased, illustrating that the hydrophobic force increased with water contact angle. Force measurements between air bubbles and sphalerite and molybdenite surfaces of different water contact angle were also conducted by Xie et al. [106, 168]. More specifically, the effect of polymer depressant (guar gum) on the bubble-molybdenite attachment was studied. When 1 ppm guar gum was added, polymer aggregates on the surface became visible from AFM images, resulting in a decreased bubble-particle attachment. Further increasing guar gum concentration to 5 ppm, the contact angle of molybdenite surface decreased from ≈74° to 65°. A monotonic repulsive force was observed. The AFM force results were consistent with the practical molybdenite flotation results. The final flotation recovery decreased from 69% to 11% and to 3% after guar gum adsorption at 1 and 5 ppm concentration solutions.

The other effective approach complementary to AFM force measurement is optical interferometry. In 2015, Shi et al. [169] first combined a reflection interference contrast microscopy (RICM) with AFM to measure the force and the thin water film profile between a bubble and mica surface simultaneously (Fig. 10). The patch was hydrophibized by thiols.

Then a bubble was attached on the end of cantilever. The dynamic profiles of air-water interface were reconstructed using RICM with nanometer resolution. It was found that the Stokes-Reynolds-Young-Laplace model can predict both the force and film drainage with a no-slip boundary condition. A stable wetting film was observed between an air bubble and a hydrophilic mica surface. In contrast, jump-in events where the interaction force drastically turned from repulsive to attractive were observed for both 45° and 90° contact angle mica surfaces (Fig. 11). Again, the critical film rupture thickness increased as contact angle increased. Due to the short range of van der Waals force and the suppression of the electrostatic force at 500 mM NaCl, an additional attractive hydrophobic force was considered as the reason for triggering film rupture. From the Stokes-Reynolds-Young-Laplace model, the effective hydrophobic decay length was 0.8 and 1.0 nm for the 45° and 90° water contact angle, respectively. These results might be explained in terms of a different water structure at the solid-water interface with different surface contact angle.

Combining AFM with RICM is a landmark in our full understanding of bubble-particle interaction [170]. In the next few years, synchronous measurement of the force and the spatiotemporal evolution of thin water film profile between bubble and particle in presence of flotation reagents will shed new light on flotation mechanism [150].

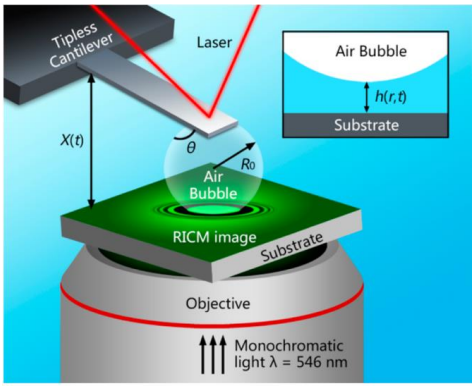

Fig. 10 Schematic of the AFM-RICM experimental setup. Adapted with permission from [169], Copyright 2015, American Chemical Society.

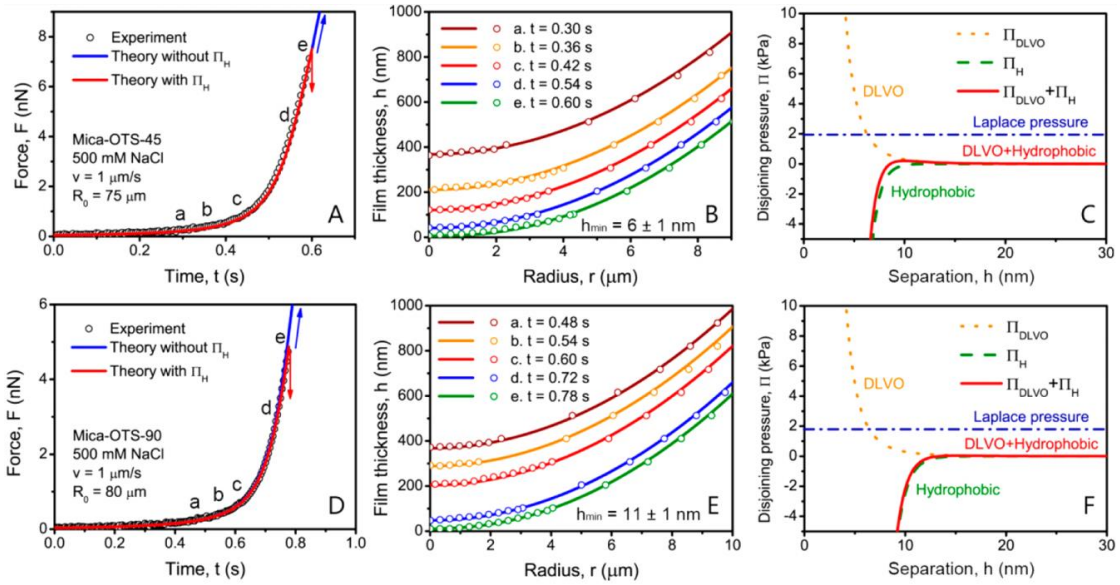

Fig. 11 Temporal evolution of the force (left), film profile (middle) and disjoining pressure (right) during approach between an air bubble and hydrophobized mica surfaces (A-C: 45° contact angle, D-E: 90° contact angle) in 500 mM NaCl solution. Open circles denote the experimental results and solid curves represent the theoretical calculation results. Adapted with permission from [169], Copyright 2015, American Chemical Society.

That a linear response for force curves is expected once a three-phase contact has been formed has recently been confirmed for the simple case of a large bubble (equal to planar surface). Based on results of James [171], Anachkov et al. [172] numerically calculated force-distance curves for a spherical particle being retracted from a planar liquid-fluid interface. With very good approximation such force curves can be described by [173]:

$$F = \frac{2\pi\gamma\delta}{0.8091 - \ln\left(R/\kappa\right)} \quad (3)$$

For a spherical particle with the contact line sliding over its surfaces when being pulled out of

the bubble, *R* is the radius. If the contact line is pinned *R* is the radius of the contact line.

7. Other applications

In recent years, it has become popular to determine the mineral surface charge and wetting characteristics using direct AFM force measurement [174]. One topic is to measure the point of zero charge (PZC) of different faces of anisotropic layered silicates such as kaolinite, talc, pyrophyllite and illite. Traditional zeta potential measurements by electrophoresis or streaming potential assume a uniform charge density on these layered silicate particles. Often, an apparent discrepancy between the macroscopic coagulation behaviour and PZC are usually observed. However, the problem can be solved using AFM. Historically, a colloid probe has usually been employed and the surface charge information was obtained by fitting the force curves with the DLVO theory. Zhao et al. [175] used an ultramicrotome cutting technique to prepare an edge surface of muscovite, while a smooth basal face was easily prepared by cleavage. A silica sphere with an 8 μm diameter was attached to the cantilever and a series of force curves were obtained. The force profiles between the silica and basal face were well fitted with classical DLVO theory. They found that pH has little effect on the surface potential of muscovite basal face. However, on the edge they could not get good results due to the roughness of the mica edge surface over the large contact area. To overcome the surface roughness effect, Gupta and Miller [43] directly used a pyramid-shaped silicon nitride tip as the probe to map the surface potential of two kaolinite basal faces (silica face and alumina face). The silicon tip was modeled as a cone with a spherical cap at its apex. Then, the DLVO forces between tip and flat surface could be reasonably approximated as the sum of the conical-substrate interaction force and the cap-substrate interaction force [176]. The

isoelectric point of the silica tetrahedral face was lower than that of the alumina octahedral face. Yan et al. [177] further used this approach to explore the surface potentials of both basal and edge faces of talc and muscovite. The ultramicrotome cutting technique was applied to prepare the edge face. The surface potentials of basal faces of both talc and muscovite were always more negatively charged than that of edge faces in the range of experimental pH (5.6-10.1) (Fig. 12). This is due to the different charging mechanisms between basal and edge faces. The permanent negative charge of basal faces is attributed to fixed isomorphic substitution while protonation-deprotonation reactions are responsible for the pH-dependent properties of the edge face. The anisotropic surface potentials of scheelite crystal and molybdenite were also studied using AFM force measurements [40, 178]. The 101 face of scheelite crystal was the most negatively charged surface, followed by 112 and 001 faces. For molybdenite, it was found that the surface potentials of both edge and basal faces are highly pH-dependent.

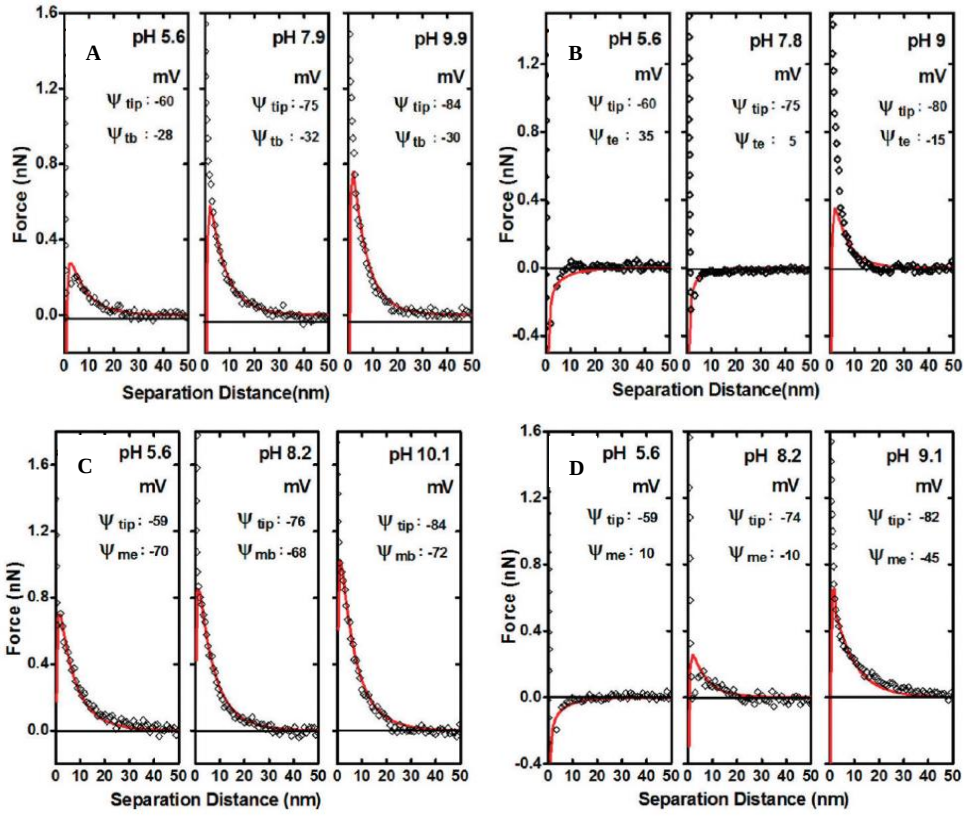

Fig. 12 Force curves between AFM tip and different faces in 1 mM KCl solution: A, talc basal plane; B, talc edge plane; C, muscovite basal plane; D, muscovite edge plane. Symbols represent experimental data and the solid lines represent theoretical fits. Adapted with permission from [177], Copyright 2011, American Chemical Society.

One can use a hydrophobized probe to map the surface hydrophobicity by fitting the force profile using extended DLVO theory with an additional hydrophobic force taken into consideration. A high attractive force corresponds to high surface hydrophobicity (local large water contact angle). Lu et al. [40] used a single exponential function to fit the experimental hydrophobic force curve between an OTS-coated tip and a molybdenite surface in 10 mM NaCl solution at various pH (Fig. 13). An attractive hydrophobic force at all pH ranges was observed. However, this was not the case between the tip and edge surface. This illustrated that the basal surface of molybdenite shows a hydrophobic character, while the edge surface is hydrophilic. This observation is consistent with the contact angle results. Xie et al. [179] adopted the same approach to map the sphalerite surface hydrophobicity before and after $CuSO_4$ activation and amyl xanthate conditioning. Amyl xanthate adsorption increased surface hydrophobicity.

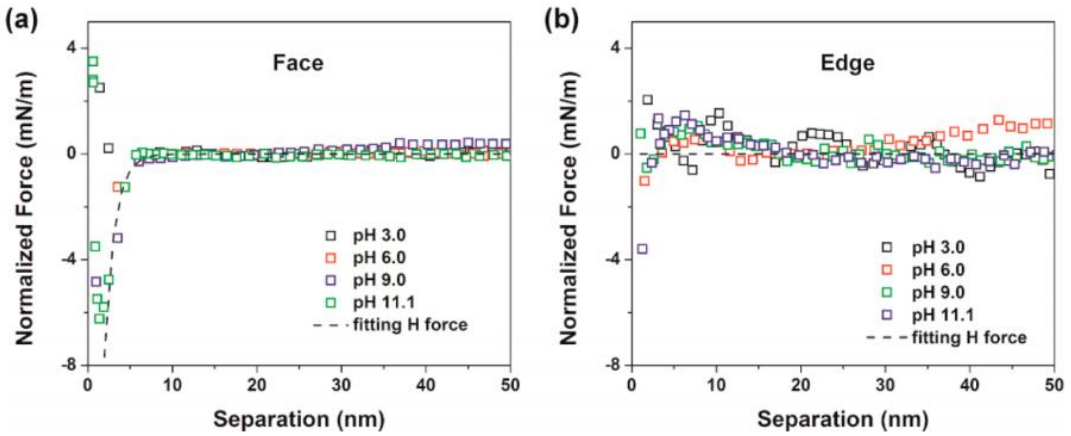

Fig. 13 Hydrophobic force between OTS-coated tip and (a) face and (b) edge of molybdenite in 10 mM NaCl solution. The dash line is the theoretical fitting result. Adapted with permission from [40], Copyright 2015, American Chemical Society.

Colloid probe AFM can also be applied to characterize hydrophobic surface heterogeneities on a micro scale. The colloid probe-sample interaction [180] and parameters derived from force-distance curves [181] in the context of flotation or other processes like filtration can be obtained. Rudolph and Peuker [182] combined hydrophobic colloid probe AFM with Raman spectroscopy to evaluate the wettability of minerals in finely inter-grown ore in situ. The mineral phase where force measurement was conducted could be identified by Raman microscopy. They proposed that adhesion force mapping is a more precise indicator for the floatability of practical minerals. The combined colloid probe AFM and Raman technique will also be a powerful tool to investigate mineral-reagent interactions in flotation systems.

8. Conclusions and perspectives

AFM is an established tool in mineral flotation used both for imaging and a surface force sensing. It can be successfully used to image the minerals, to characterize the water structure at mineral-water interface, to study the adsorption of flotation reagent on mineral surfaces, to measure inter-particle force directly, and bubble-particle interaction. Detailed information at a nanoscale has been obtained, greatly assisting the fundamental understanding of flotation. One challenge is to measure precise shapes of water/air interfaces in particle-bubble experiments due to the absence of hard contact point. The main drawback of AFM is the absence of a chemical imaging capability. It is necessary to develop new AFM-based techniques have the ability to analyze both surface morphology and chemical composition in

the contact area. Optical spectroscopy analysis will be the optimal choice. Recently, significant progress has been achieved on the combination of AFM and infrared spectroscopy(IR) [183]. The AFM tip itself acts as the IR detector and thus can overcome the spatial resolution limits of conventional IR due to the existence of optical diffraction limitation (Fig. 14). In this context, more complementary information on mineral surface/mineral-water interface can be obtained. For example, the specific adsorption of flotation reagents on mineral surface can be identified successfully. However, tip-enhanced IR spectroscopy is difficult to operate in aqueous medium due to the strong IR absorption bands of water. In conclusion, the complementary characterization of chemical composition using optical spectroscopy for AFM topography imaging and the synchronous measurement of the force and distance involving deformable bubble as a force sensor will become an active area over the coming years and further shed new light on flotation mechanism.

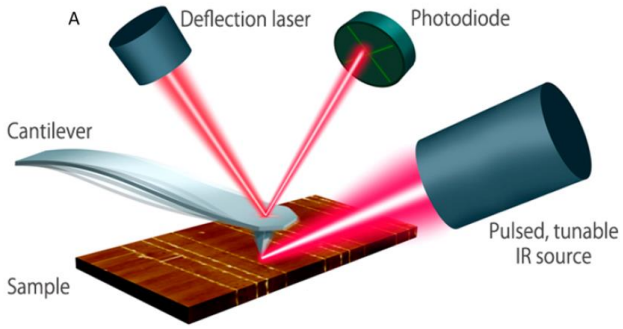

Fig. 14 Schematic diagram of AFM-IR. IR laser is focused on a sample near the tip of an AFM. The AFM tip is used as a local detector of IR absorption. Adapted with permission from [183], Copyright 2016, American Chemical Society.

Acknowledgments

This research was supported by the National Nature Science Foundation of China (grant no. 51774286, 51574236), a project funded by the China Postdoctoral Science Foundation

(2015T80606, 2014M550317) for which the authors express their appreciation. Yaowen Xing also appreciates China Scholarship Council for the financial support for his research stay at Max Planck Institute for Polymer Research. Hans-Jürgen Butt also acknowledges support by the Max Planck Center for Complex Fluid Dynamics Fluid Dynamics of Complexity.

References

[1] Binnig G, Quate CF, Gerber C. Atomic force microscope. Physical Review Letters. 1986;56: 930-933.

[2] Drake B, Prater CB, Weisenhorn AL, Gould SAC, Albrecht TR, Quate CF, Cannell DS, Hansma HG, Hansma PK. Imaging crystals, polymers, and processes in water with the atomic force microscope. Science. 1989;243:1586-1589.

[3] Butt HJ, Berger R, Bonaccurso E, Chen Y, Wang J. Impact of atomic force microscopy on interface and colloid science. Advances in Colloid and Interface Science. 2007;133:91-104.

[4] Ducker WA, Senden TJ, Pashley RM. Direct measurement of colloidal forces using an atomic force microscope. Nature. 1991;353:239.

[5] Butt HJ. Measuring electrostatic, van der Waals, and hydration forces in electrolyte solutions with an atomic force microscope. Biophysical Journal. 1991;60:1438-1444.

[6] Butt HJ, Cappella B, Kappl M. Force measurements with the atomic force microscope: Technique, interpretation and applications. Surface Science Reports. 2005;59:1-152.

[7] Bowen WR, Hilal N. Atomic force microscopy in process engineering: an introduction to AFM for improved processes and products: Butterworth-Heinemann; 2009.

[8] Nguyen AV, Schulze HJ. Colloidal Science of Flotation. New York, America: Marcel Dekker Inc; 2004.

[9] Ejtemaei M, Gharabaghi M, Irannajad M. A review of zinc oxide mineral beneficiation using flotation method. Advances in Colloid and Interface Science. 2014;206:68-78.

[10] Aghazadeh S, Mousavinezhad SK, Gharabaghi M. Chemical and colloidal aspects of collectorless flotation behavior of sulfide and non-sulfide minerals. Advances in Colloid and Interface Science. 2015;225:203-217.

[11] Wu ZJ, Wang XM, Liu HN, Zhang HF, Miller JD. Some physicochemical aspects of water-soluble mineral flotation. Advances in Colloid and Interface Science. 2016;235:190-200.

[12] Xing YW, Gui XH, Liu JT, Cao YJ, Lu Y. Effects of energy input on the laboratory column flotation of fine coal. Separation Science Technology. 2015;50:2559-2567.

[13] Xing YW, Gui XH, Cao YJ, Wang DP, Zhang HJ. Clean low-rank-coal purification technique combining cyclonic-static microbubble flotation column with collector emulsification. Journal of Cleaner Production. 2017; 153:657-672.

[14] Xing YW, Gui XH, Cao YJ, Wang YW, Xu MD, Wang DY, et al. Effect of compound collector and blending frother on froth stability and flotation performance of oxidized coal. Powder Technology. 2017;305:166-173.

[15] Rubio J, Souza ML, Smith RW. Overview of flotation as a wastewater treatment technique. Minerals Engineering, 2002;15:139-155

[16] Cai X, Chen J, Liu M, Ji Y, An S. Numerical studies on dynamic characteristics of oil-water separation in loop flotation column using a population balance model. Separation and Purification Technology. 2017;176:134-144.

[17] Rao F, Liu Q. Froth treatment in athabasca oil sands bitumen recovery process: a review. Energy & Fuels. 2013;27:7199-7207

[18] Kasongo T, Zhou Z, Xu Z, Masliyah J. Effect of clays and calcium ions on bitumen extraction from Athabasca oil sands using flotation. The Canadian Journal of Chemical Engineering. 2000;78:674-681.

[19] Zhou F, Yan C, Wang H, Zhou S, Liang H. The result of surfactants on froth flotation of unburned carbon from coal fly ash. Fuel. 2017;190:182-188.

[20] Altun NE, Xiao CF, Hwang JY. Separation of unburned carbon from fly ash using a concurrent flotation column. Fuel Processing Technology. 2009;90:1464-1470.

[21] Bartonova L. Unburned carbon from coal combustion ash: An overview. Fuel Processing Technology. 2015;134:136-158.

[22] Finch JA, Hardie CA. An example of innovation from the waste management industry: Deinking flotation cells. Minerals Engineering. 1999;12:467-475.

[23] Vashisth S, Bennington CPJ, Grace JR, Kerekes RJ. Column flotation deinking: State-of-the-art and opportunities. Resources, Conservation and Recycling. 2011;55:1154-1177.

[24] Chau T, Bruckard W, Koh P, Nguyen A. A review of factors that affect contact angle and implications for flotation practice. Advances in Colloid and Interface Science. 2009;150:106-115.

[25] Hosseini S, Forssberg E. XPS & FTIR study of adsorption characteristics using cationic and anionic collectors on smithsonite. Journal of Minerals and Materials Characterization and Engineering. 2006;5:21-45.

[26] Beattie DA, Kempson IM, Fan LJ, Skinner WM. Synchrotron XPS studies of collector adsorption and co-adsorption on gold and gold: silver alloy surfaces. International Journal of Mineral Processing. 2009;92:162-168.

[27] Giesekke E. A review of spectroscopic techniques applied to the study of interactions between minerals and reagents in flotation systems. International Journal of Mineral Processing. 1983;11:19-56.

[28] Hosseinpour S, Tang FJ, Wang FL, Livingstone RA, Schlegel SJ, Ohto T, et al. Chemisorbed and Physisorbed Water at the TiO2/Water Interface. Journal of Physical Chemistry Letters. 2017;8:2195-2199.

[29] Schaefer J, Gonella G, Bonn M, Backus EHG. Surface-specific vibrational spectroscopy of the water/silica interface: screening and interference. Physical Chemistry Chemical Physics. 2017;19:16875-16880.

[30] Xu Z, Liu J, Choung J, Zhou Z. Electrokinetic study of clay interactions with coal in flotation. International Journal of Mineral Processing. 2003;68:183-196.

[31] Liu J, Zhou Z, Xu Z, Masliyah J. Bitumen–clay interactions in aqueous media studied by zeta potential distribution measurement. Journal of Colloid and Interface Science. 2002;252:409-418.

[32] Wu C, Wang L, Harbottle D, Masliyah J, Xu Z. Studying bubble–particle interactions by zeta potential distribution analysis. Journal of Colloid and Interface Science. 2015;449:399-408.

[33] Ralston J, Fornasiero D, Hayes R. Bubble–particle attachment and detachment in flotation. International Journal of Mineral Processing. 1999;56:133-164.

[34] Nguyen A, Evans G, Schulze H. Prediction of van der Waals interaction in bubble–particle attachment in flotation. International Journal of Mineral Processing. 2001;61:155-169.

[35] Dai Z, Fornasiero D, Ralston J. Particle–bubble collision models-a review. Advances in

Colloid and Interface Science. 2000;85:231-256.

[36] Koh P, Schwarz M. CFD modelling of bubble–particle collision rates and efficiencies in a flotation cell. Minerals Engineering. 2003;16:1055-1059.

[37] Leiro J, Torhola M, Laajalehto K. The AFM method in studies of muscovite mica and galena surfaces. Journal of Physics and Chemistry of Solids. 2017;100:40-44.

[38] Beaussart A, Parkinson L, Mierczynska-Vasilev A, Beattie DA. Adsorption of modified dextrins on molybdenite: AFM imaging, contact angle, and flotation studies. Journal of Colloid and Interface Science. 2012;368:608-615.

[39] Xie L, Wang J, Shi C, Huang J, Zhang H, Liu Q, Zeng HB. Probing surface interactions of electrochemically active galena mineral surface using atomic force microscopy. The Journal of Physical Chemistry C. 2016;120:22433-22442.

[40] Lu Z, Liu Q, Xu Z, Zeng H. Probing anisotropic surface properties of molybdenite by direct force measurements. Langmuir. 2015;31:11409-11418.

[41] Gupta V, Hampton MA, Nguyen AV, Miller JD. Crystal lattice imaging of the silica and alumina faces of kaolinite using atomic force microscopy. Journal of Colloid and Interface Science. 2010;352:75-80.

[42] Hampton MA, Plackowski C, Nguyen AV. Physical and chemical analysis of elemental sulfur formation during galena surface oxidation. Langmuir. 2011;27:4190-4201.

[43] Gupta V, Miller JD. Surface force measurements at the basal planes of ordered kaolinite particles. Journal of Colloid and Interface Science. 2010;344:362-371.

[44] Bruening F, Cohen A. Measuring surface properties and oxidation of coal macerals using the atomic force microscope. International Journal of Coal Geology. 2005;63:195-204.

[45] Morga R. Changes of semifusinite and fusinite surface roughness during heat treatment

determined by atomic force microscopy. International Journal of Coal Geology. 2011;88:218-226.

[46] Pan JN, Zhu HT, Hou QL, Wang HC, Wang S. Macromolecular and pore structures of Chinese tectonically deformed coal studied by atomic force microscopy. Fuel. 2015;139:94-101.

[47] Wu D, Liu GJ, Sun RY, Chen SC. Influences of magmatic intrusion on the macromolecular and pore structures of coal: Evidences from Raman spectroscopy and atomic force microscopy. Fuel. 2014;119:191-201.

[48] Drosthansen W. Effects of vicinal water on colloidal stability and sedimentation processes. Journal of Colloid and Interface Science. 1977;58:251-262.

[49] Du H, Miller JD. A molecular dynamics simulation study of water structure and adsorption states at talc surfaces. International Journal of Mineral Processing. 2007;84:172-184.

[50] Gao J, Szoszkiewicz R, Landman U, Riedo E. Structured and viscous water in subnanometer gaps. Physical Review B. 2007;75:115415.

[51] Fenter P, Lee SS. Hydration layer structure at solid-water interfaces. MRS Bulletin. 2014;39:1056-1061.

[52] Marutschke C, Walters D, Cleveland J, Hermes I, Bechstein R, Kühnle A. Three-dimensional hydration layer mapping on the (10.4) surface of calcite using amplitude modulation atomic force microscopy. Nanotechnology. 2014;25:335703.

[53] Miyazawa K, Watkins M, Shluger A, Fukuma T. Influence of ions on two-dimensional and three-dimensional atomic force microscopy at fluorite-water interfaces. Nanotechnology. 2017;28:245701.

[54] Raviv U, Laurat P, Klein J. Fluidity of water confined to subnanometre films. Nature. 2001;413:51-54.

[55] Raviv U, Perkin S, Laurat P, Klein J. Fluidity of water confined down to subnanometer films. Langmuir. 2004;20:5322-5332.

[56] Fukuma T, Reischl B, Kobayashi N, Spijker P, Canova FF, Miyazawa K, Foster A. Mechanism of atomic force microscopy imaging of three-dimensional hydration structures at a solid-liquid interface. Physical Review B. 2015;92:155412.

[57] Mezger M, Reichert H, Schöder S, Okasinski J, Schröder H, Dosch H, Palms D, Ralston J, Honkimäki V. High-resolution in situ x-ray study of the hydrophobic gap at the water-octadecyl-trichlorosilane interface. Proceedings of the National Academy of Sciences. 2006;103:18401-18404.

[58] Doshi DA, Watkins EB, Israelachvili JN, Majewski J. Reduced water density at hydrophobic surfaces: Effect of dissolved gases. Proceedings of the National Academy of Sciences. 2005;102:9458-9462.

[59] Jensen TR, Jensen MØ, Reitzel N, Balashev K, Peters GH, Kjaer K, Bjørnholm T. Water in contact with extended hydrophobic surfaces: Direct evidence of weak dewetting. Physical Review Letters. 2003;90:086101.

[60] Fukuma T, Kobayashi K, Matsushige K, Yamada H. True atomic resolution in liquid by frequency-modulation atomic force microscopy. Applied Physics Letters. 2005;87:034101.

[61] Israelachvili JN, Pashley RM. Molecular layering of water at surfaces and origin of repulsive hydration forces. Nature. 1983;306:249-250.

[62] Zachariah Z, Espinosa-Marzal RM, Spencer ND, Heuberger MP. Stepwise collapse of highly overlapping electrical double layers. Physical Chemistry Chemical Physics.

2016;18:24417-24427.

[63] Fukuma T, Ueda Y, Yoshioka S, Asakawa H. Atomic-scale distribution of water molecules at the mica-water interface visualized by three-dimensional scanning force microscopy. Physical Review Letters. 2010;104:016101.

[64] Imada H, Kimura K, Onishi H. Water and 2-propanol structured on calcite (104) probed by frequency-modulation atomic force microscopy. Langmuir. 2013;29:10744-10751.

[65] Songen H, Marutschke C, Spijker P, Holmgren E, Hermes I, Bechstein R, Klassen S, Tracey T, Foster A, Kühnle A . Chemical identification at the solid-liquid interface. Langmuir. 2017;33:125-129.

[66] Watkins M, Shluger AL. Mechanism of contrast formation in atomic force microscopy in water. Physical Review Letters. 2010;105: 196101.

[67] Miyazawa K, Kobayashi N, Watkins M, Shluger AL, Amano K, Fukuma T. A relationship between three-dimensional surface hydration structures and force distribution measured by atomic force microscopy. Nanoscale. 2016;8:7334-7342.

[68] Fukuma T, Onishi K, Kobayashi N, Matsuki A, Asakawa H. Atomic-resolution imaging in liquid by frequency modulation atomic force microscopy using small cantilevers with megahertz-order resonance frequencies. Nanotechnology. 2012;23: 135706.

[69] Songen H, Nalbach M, Adam H, Kuhnle A. Three-dimensional atomic force microscopy mapping at the solid-liquid interface with fast and flexible data acquisition. Review of Scientific Instruments. 2016;87: 063704.

[70] Schubert H. Nanobubbles, hydrophobic effect, heterocoagulation and hydrodynamics in flotation. International Journal of Mineral Processing. 2005;78:11-21.

[71] Sobhy A, Tao D. Nanobubble column flotation of fine coal particles and associated

fundamentals. International Journal of Mineral processing. 2013;124:109-116.

[72] Parker J, Claesson P, Attard P. Bubbles, cavities, and the long-ranged attraction between hydrophobic surfaces. Journal of Physical Chemistry. 1994;98:8468-8480.

[73] Ishida N, Inoue T, Miyahara M, Higashitani K. Nano bubbles on a hydrophobic surface in water observed by tapping-mode atomic force microscopy. Langmuir. 2000;16:6377-6380.

[74] Lou ST, Ouyang ZQ, Zhang Y, Li XJ, Hu J, Li MQ, Yang FJ. Nanobubbles on solid surface imaged by atomic force microscopy. Journal of Vacuum Science & Technology B: Microelectronics and Nanometer Structures Processing, Measurement, and Phenomena. 2000;18:2573-2575.

[75] Peng H, Hampton MA, Nguyen AV. Nanobubbles do not sit alone at the solid-liquid interface. Langmuir. 2013;29:6123-6130.

[76] Zhang XH, Maeda N, Craig VSJ. Physical properties of nanobubbles on hydrophobic surfaces in water and aqueous solutions. Langmuir. 2006;22:5025-5035.

[77] Walczyk W, Schönherr H. Dimensions and the profile of surface nanobubbles: tip–nanobubble interactions and nanobubble deformation in atomic force microscopy. Langmuir. 2014;30:11955-11965.

[78] Walczyk W, Schon PM, Schönherr H. The effect of PeakForce tapping mode AFM imaging on the apparent shape of surface nanobubbles. Journal of Physics: Condensed Matter. 2013;25:184005.

[79] Ko HC, Hsu WH, Yang CW, Fang CK, Lu YH, Hwang IS. High-resolution characterization of preferential gas adsorption at the graphene-water interface. Langmuir. 2016;32:11164-11171.

[80] Walczyk W, Schönherr H. Characterization of the interaction between AFM tips and

surface nanobubbles. Langmuir. 2014;30:7112-7126.

[81] Zhao B, Song Y, Wang S, Dai B, Zhang L, Dong Y, Lü J, Hu J. Mechanical mapping of nanobubbles by PeakForce atomic force microscopy. Soft Matter. 2013;9:8837-8843.

[82] Schönherr H, Hain N, Walczyk W, Wesner D, Druzhinin SI. Surface nanobubbles studied by atomic force microscopy techniques: Facts, fiction, and open questions. Japanese Journal of Applied Physics. 2016; 55:08NA01.

[83] Zhang XH, Khan A, Ducker WA. A nanoscale gas state. Physical Review Letters. 2007;98:136101.

[84] Miller JD, Hu YH, Veeramasuneni S, Lu YQ. In-situ detection of butane gas at a hydrophobic silicon surface. Colloids and Surfaces A: Physicochemical and Engineering Aspects. 1999;154:137-147.

[85] Chan CU, Ohl CD. Total-internal-reflection-fluorescence microscopy for the study of nanobubble dynamics. Physical Review Letters. 2012;109:174501.

[86] Li M, Tonggu L, Zhan X, Mega TL, Wang L. Cryo-EM visualization of nanobubbles in aqueous solutions. Langmuir. 2016;32:11111-11115.

[87] Switkes M, Ruberti J. Rapid cryofixation/freeze fracture for the study of nanobubbles at solid–liquid interfaces. Applied Physics Letters. 2004;84:4759-4761.

[88] Zhang XH. Quartz crystal microbalance study of the interfacial nanobubbles. Physical Chemistry Chemical Physics. 2008;10:6842-6848.

[89] Hain N, Wesner D, Druzhinin SI, Schönherr H. Surface nanobubbles studied by time-resolved fluorescence microscopy methods combined with AFM: The impact of surface treatment on nanobubble nucleation. Langmuir. 2016;32:11155-11163.

[90] Pan G, He G, Zhang M, Zhou Q, Tyliszczak T, Tai R, et al. Nanobubbles at hydrophilic

particle-water interfaces. Langmuir. 2016;32:11133-11137.

[91] Palmer LA, Cookson D, Lamb RN. The relationship between nanobubbles and the hydrophobic force. Langmuir. 2011;27:144-147.

[92] Alheshibri M, Qian J, Jehannin M, Craig VS. A history of nanobubbles. Langmuir. 2016;32:11086-11100.

[93] Zhang XH, Chan DYC, Wang DY, Maeda N. Stability of interfacial nanobubbles. Langmuir. 2013;29:1017-1023.

[94] Lohse D, Zhang XH. Surface nanobubbles and nanodroplets. Reviews of Modern Physics. 2015; 87:981.

[95] Zhang XH, Zhang XD, Lou ST, Zhang ZX, Sun JL, Hu J. Degassing and temperature effects on the formation of nanobubbles at the mica/water interface. Langmuir. 2004;20(9):3813-3815.

[96] Zhang XH, Zhang X, Sun J, Zhang Z, Li G, Fang H, Xiao X, Zeng X, Hu J. Detection of novel gaseous states at the highly oriented pyrolytic graphite-water interface. Langmuir. 2007;23:1778-1783.

[97] van Limbeek MA, Seddon JR. Surface nanobubbles as a function of gas type. Langmuir. 2011;27:8694-8699.

[98] Zhang X, Uddin MH, Yang H, Toikka G, Ducker W, Maeda N. Effects of surfactants on the formation and the stability of interfacial nanobubbles. Langmuir. 2012;28:10471-10477.

[99] Xu C, Peng S, Qiao GG, Gutowski V, Lohse D, Zhang X. Nanobubble formation on a warmer substrate. Soft Matter. 2014;10:7857-7864.

[100] Seiedi O, Rahbar M, Nabipour M, Emadi MA, Ghatee MH, Ayatollahi S. Atomic force microscopy (AFM) investigation on the surfactant wettability alteration mechanism of aged

mica mineral surfaces. Energy & Fuels. 2010;25:183-188.

[101] Fielden ML, Claesson PM, Verrall RE. Investigating the adsorption of the gemini surfactant “12-2-12” onto mica using atomic force microscopy and surface force apparatus measurements. Langmuir. 1999;15:3924-3934.

[102] Dong J, Mao G. Direct study of $C_{12}E_5$ aggregation on mica by atomic force microscopy imaging and force measurements. Langmuir. 2000;16:6641-6647.

[103] Ferrari M, Ravera F, Viviani M, Liggieri L. Characterization of surfactant aggregates at solid–liquid surfaces by atomic force microscopy. Colloids and Surfaces A: Physicochemical and Engineering Aspects. 2004;249:63-67.

[104] Chennakesavulu K, Raju GB, Prabhakar S, Nair CM, Murthy K. Adsorption of oleate on fluorite surface as revealed by atomic force microscopy. International Journal of Mineral Processing. 2009;90:101-104.

[105] Paiva P, Monte M, Simao R, Gaspar J. In situ AFM study of potassium oleate adsorption and calcium precipitate formation on an apatite surface. Minerals Engineering. 2011;24:387-395.

[106] Xie L, Wang J, Yuan D, Shi C, Cui X, Zhang H, Liu Q, Liu QX, Zeng H. Interaction mechanisms between air bubble and molybdenite surface: Impact of solution salinity and polymer adsorption. Langmuir. 2017;33:2353-2361.

[107] Mierczynska-Vasilev A, Beattie DA. Adsorption of tailored carboxymethyl cellulose polymers on talc and chalcopyrite: Correlation between coverage, wettability, and flotation. Minerals Engineering. 2010;23:985-993.

[108] Rief M, Oesterhelt F, Heymann B, Gaub HE. Single molecule force spectroscopy on polysaccharides by atomic force microscopy. Science. 1997;275:1295-1297.

[109] Neuman KC, Nagy A. Single-molecule force spectroscopy: optical tweezers, magnetic tweezers and atomic force microscopy. Nature methods. 2008;5:491-505.

[110] Liu C, Shi W, Cui S, Wang Z, Zhang X. Force spectroscopy of polymers: Beyond single chain mechanics. Current Opinion in Solid State and Materials Science. 2005;9:140-148.

[111] Zhang X, Liu C, Wang Z. Force spectroscopy of polymers: Studying on intramolecular and intermolecular interactions in single molecular level. Polymer. 2008;49:3353-3361.

[112] Hugel T, Grosholz M, Clausen-Schaumann H, Pfau A, Gaub H, Seitz M. Elasticity of single polyelectrolyte chains and their desorption from solid supports studied by AFM based single molecule force spectroscopy. Macromolecules. 2001;34:1039-1047.

[113] Long J, Xu Z, Masliyah JH. Adhesion of single polyelectrolyte molecules on silica, mica, and bitumen surfaces. Langmuir. 2006;22:1652-1659.

[114] Sun W, Long J, Xu Z, Masliyah JH. Study of $Al(OH)_3$-polyacrylamide-induced pelleting flocculation by single molecule force spectroscopy. Langmuir. 2008;24:14015-14021.

[115] Pensini E, Yip CM, O'Carroll D, Sleep BE. Carboxymethyl cellulose binding to mineral substrates: Characterization by atomic force microscopy–based Force spectroscopy and quartz-crystal microbalance with dissipation monitoring. Journal of Colloid and Interface Science. 2013;402:58-67.

[116] Fa K, Nguyen AV, Miller JD. Interaction of calcium dioleate collector colloids with calcite and fluorite surfaces as revealed by AFM force measurements and molecular dynamics simulation. International Journal of Mineral Processing. 2006;81:166-177.

[117] Fa K, Jiang T, Nalaskowski J, Miller JD. Interaction forces between a calcium dioleate sphere and calcite/fluorite surfaces and their significance in flotation. Langmuir. 2003;19:10523-10530.

[118] Free ML, Miller JD. Kinetics of 18-carbon carboxylate adsorption at the fluorite surface. Langmuir. 1997;13:4377-4382.

[119] Xing Y, Li C, Gui X, Cao Y. Interaction forces between paraffin/stearic acid and fresh/oxidized coal particles measured by atomic force microscopy. Energy & Fuels. 2017;31:3305-3312.

[120] Israelachvili J, Pashley R. The hydrophobic interaction is long-range, decaying exponentially with distance. Nature. 1982;300:341-342.

[121] Israelachvili JN, Pashley RM. Measurement of the hydrophobic interaction between two hydrophobic surfaces in aqueous electrolyte solutions. Journal of Colloid and Interface Science. 1984;98:500-514.

[122] Rabinovich YI, Yoon RH. Use of atomic-force microscope for the measurements of hydrophobic forces between silanated silica plate and glass sphere. Langmuir. 1994;10:1903-1909.

[123] Christenson HK, Claesson PM. Direct measurements of the force between hydrophobic surfaces in water. Advances in Colloid and Interface Science. 2001;91:391-436.

[124] Tyrrell JWG, Attard P. Atomic force microscope images of nanobubbles on a hydrophobic surface and corresponding force-separation data. Langmuir. 2002;18:160-167.

[125] Hampton MA, Nguyen AV. Systematically altering the hydrophobic nanobubble bridging capillary force from attractive to repulsive. Journal of Colloid and Interface Science. 2009;333:800-806.

[126] Hampton MA, Donose BC, Nguyen AV. Effect of alcohol-water exchange and surface scanning on nanobubbles and the attraction between hydrophobic surfaces. Journal of Colloid and Interface Science. 2008;325:267-274.

[127] Christensen H, Claesson P. Cavitation and the interaction between macroscopic surfaces. Science. 1988;239:390-392.

[128] Meyer EE, Rosenberg KJ, Israelachvili J. Recent progress in understanding hydrophobic interactions. Proceedings of the National Academy of Sciences. 2006;103:15739-15746.

[129] Xing YW, Gui XH, Cao YJ. Effect of calcium ion on coal flotation in the presence of kaolinite clay. Energy & Fuels. 2016;30:1517-1523.

[130] Gui XH, Xing YW, Rong GQ, Cao YJ, Liu JT. Interaction forces between coal and kaolinite particles measured by atomic force microscopy. Powder Technology. 2016;301:349-355.

[131] Xing YW, Xu XH, Gui XH, Cao YJ, Xu MD. Effect of kaolinite and montmorillonite on fine coal flotation. Fuel. 2017;195:284-289.

[132] Borkovec M, Papastavrou G. Interactions between solid surfaces with adsorbed polyelectrolytes of opposite charge. Current Opinion in Colloid & Interface Science. 2008;13:429-237.

[133] Borkovec M, Szilagyi I, Popa I, Finessi M, Sinha P, Maroni P, et al. Investigating forces between charged particles in the presence of oppositely charged polyelectrolytes with the multi-particle colloidal probe technique. Advances in Colloid and Interface Science. 2012;179:85-98.

[134] Abraham T, Christendat D, Xu Z, Masliyah J, Gohy J-F, Jérôme R. Role of polyelectrolyte charge density in tuning colloidal forces. AIChE Journal. 2004;50:2613-2626.

[135] Zhou Y, Gan Y, Wanless EJ, Jameson GJ, Franks GV. Interaction forces between silica surfaces in aqueous solutions of cationic polymeric flocculants: effect of polymer charge.

Langmuir. 2008;24:10920-10928.

[136] Ofori P, Nguyen AV, Firth B, McNally C, Hampton MA. The role of surface interaction forces and mixing in enhanced dewatering of coal preparation tailings. Fuel. 2012;97:262-268.

[137] Ruiz-Cabello FJM, Maroni P, Borkovec M. Direct measurements of forces between different charged colloidal particles and their prediction by the theory of Derjaguin, Landau, Verwey, and Overbeek (DLVO). The Journal of Chemical Physics. 2013;138:234705.

[138] Ivanova NO, Xu Z, Liu Q, Masliyah JH. Surface forces in unconventional oil processing. Current Opinion in Colloid & Interface Science. 2017;27:63-73.

[139] Masliyah J, Czarnecki J, Xu Z. Handbook on theory and practice of bitumen recovery from Athabasca oil sands. Theoretical Basis. 2011;1.

[140] Liu J, Xu Z, Masliyah J. Interaction forces in bitumen extraction from oil sands. Journal of Colloid and Interface Science. 2005;287:507-520.

[141] Long J, Drelich J, Xu Z, Masliyah JH. Effect of operating temperature on water-based oil sands processing. The Canadian Journal of Chemical Engineering. 2007;85:726-738.

[142] Zhang Y, Ding M, Liu J, Jia W, Ren S. Studies on bitumen–silica interaction in surfactants and divalent cations solutions by atomic force microscopy. Colloids and Surfaces A: Physicochemical and Engineering Aspects. 2015;482:241-247.

[143] Liu J, Xu Z, Masliyah J. Role of fine clays in bitumen extraction from oil sands. AIChE Journal. 2004;50:1917-1927.

[144] Diao M, Taran E, Mahler S, Nguyen AV. A concise review of nanoscopic aspects of bioleaching bacteria-mineral interactions. Advances in Colloid and Interface Science. 2014;212:45-63.

[145] Meyer RL, Zhou X, Tang L, Arpanaei A, Kingshott P, Besenbacher F. Immobilisation of living bacteria for AFM imaging under physiological conditions. Ultramicroscopy. 2010;110:1349-1357.

[146] Bowen WR, Hilal N, Lovitt RW, Wright CJ. Direct measurement of the force of adhesion of a single biological cell using an atomic force microscope. Colloids and Surfaces A: Physicochemical and Engineering Aspects. 1998;136:231-234.

[147] Lower SK, Tadanier CJ, Hochella MF. Measuring interfacial and adhesion forces between bacteria and mineral surfaces with biological force microscopy. Geochimica et Cosmochimica Acta. 2000;64:3133-3139.

[148] Diao M, Nguyen TA, Taran E, Mahler S, Nguyen AV. Differences in adhesion of A. thiooxidans and A. ferrooxidans on chalcopyrite as revealed by atomic force microscopy with bacterial probes. Minerals Engineering. 2014;61:9-15.

[149] Xing Y, Gui X, Cao Y. The hydrophobic force for bubble-particle attachment in flotation-a brief review. Physical Chemistry Chemical Physics. 2017. DOI: 10.1039/C7CP03856A.

[150] Xing Y, Gui X, Pan L, Pinchasik B-E, Cao Y, Liu J, Kappl K, Butt HJ. Recent experimental advances for understanding bubble-particle attachment in flotation. Advances in Colloid and Interface Science. 2017; 246:105-132.

[151] Chan DY, Klaseboer E, Manica R. Theory of non-equilibrium force measurements involving deformable drops and bubbles. Advances in Colloid and Interface Science. 2011;165:70-90.

[152] Ducker WA, Xu Z, Israelachvili JN. Measurements of hydrophobic and DLVO forces in bubble-surface interactions in aqueous solutions. Langmuir. 1994;10:3279-3289.

[153] Butt H-J. A technique for measuring the force between a colloidal particle in water and a bubble. Journal of Colloid and Interface Science. 1994;166:109-117.

[154] Tabor RF, Grieser F, Dagastine RR, Chan DY. Measurement and analysis of forces in bubble and droplet systems using AFM. Journal of Colloid and Interface Science. 2012;371:1-14.

[155] Johnson DJ, Miles NJ, Hilal N. Quantification of particle-bubble interactions using atomic force microscopy: A review. Advances in Colloid and Interface Science. 2006;127:67-81.

[156] Nguyen AV, Nalaskowski J, Miller JD. A study of bubble-particle interaction using atomic force microscopy. Minerals Engineering. 2003;16:1173-1181.

[157] Nguyen AV, Evans GM, Nalaskowski J, Miller JD. Hydrodynamic interaction between an air bubble and a particle: atomic force microscopy measurements. Experimental Thermal and Fluid Science. 2004;28:387-394.

[158] Ishida N. Direct measurement of hydrophobic particle-bubble interactions in aqueous solutions by atomic force microscopy: Effect of particle hydrophobicity. Colloids and Surfaces A: Physicochemical and Engineering Aspects. 2007;300:293-299.

[159] Fielden ML, Hayes RA, Ralston J. Surface and capillary forces affecting air bubble−particle interactions in aqueous electrolyte. Langmuir. 1996;12:3721-727.

[160] Englert A, Krasowska M, Fornasiero D, Ralston J, Rubio J. Interaction force between an air bubble and a hydrophilic spherical particle in water, measured by the colloid probe technique. International Journal of Mineral Processing. 2009;92:121-127.

[161] Taran E, Hampton MA, Nguyen AV, Attard P. Anomalous time effect on particle-bubble interactions studied by atomic force microscopy. Langmuir. 2009;25:2797-2803.

[162] Preuss M, Butt H-J. Direct measurement of particle-bubble interactions in aqueous electrolyte: Dependence on surfactant. Langmuir. 1998;14:3164-3174.

[163] Preuss M, Butt HJ. Direct measurement of forces between particles and bubbles. International Journal of Mineral Processing. 1999;56:99-115.

[164] Assemi S, Nguyen AV, Miller JD. Direct measurement of particle–bubble interaction forces using atomic force microscopy. International Journal of Mineral Processing. 2008;89:65-70.

[165] Chan DY, Manor O, Connor JN, Horn RG. Soft matter: from shapes to forces on the nanoscale. Soft Matter. 2008;4:471-474.

[166] Manica R, Hendrix MHW, Gupta R, Klaseboer E, Ohl CD, Chan DYC. Effects of hydrodynamic film boundary conditions on bubble-wall impact. Soft Matter. 2013;9:9755-9758.

[167] Shi C, Chan DYC, Liu QX, Zeng HB. Probing the hydrophobic interaction between air bubbles and partially hydrophobic surfaces using atomic force microscopy. The Journal of Physical Chemistry C. 2014;118:25000-25008.

[168] Xie L, Shi C, Wang J, Huang J, Lu Q, Liu Q, Zeng H. Probing the interaction between air bubble and sphalerite mineral surface using atomic force microscope. Langmuir. 2015;31:2438-2446.

[169] Shi C, Cui X, Xie L, Liu QX, Chan DYC, Israelachvili JN, Zeng H. Measuring forces and spatiotemporal evolution of thin water films between an air bubble and solid surfaces of different hydrophobicity. ACS Nano. 2015;9:95-104.

[170] Schönherr H. Forces and thin water film drainage in deformable asymmetric nanoscale contacts. ACS Nano. 2015;9:12-15.

[171] James DF. The meniscus on the outside of a small circular cylinder. Journal of Fluid Mechanics. 1974;63:657-664.

[172] Anachkov SE, Lesov I, Zanini M, Kralchevsky PA, Denkov ND, Isa L. Particle detachment from fluid interfaces: theory vs. experiments. Soft Matter. 2016;12:7632-7643.

[173] Butt H-J, Gao N, Papadopoulos P, Steffen W, Kappl M, Berger Rd. Energy dissipation of moving drops on superhydrophobic and superoleophobic surfaces. Langmuir. 2016;33:107-116.

[174] Yin X, Gupta V, Du H, Wang X, Miller JD. Surface charge and wetting characteristics of layered silicate minerals. Advances in Colloid and Interface Science. 2012;179:43-50.

[175] Zhao H, Bhattacharjee S, Chow R, Wallace D, Masliyah JH, Xu Z. Probing surface charge potentials of clay basal planes and edges by direct force measurements. Langmuir. 2008;24:12899-12910.

[176] Drelich J, Long J, Yeung A. Determining surface potential of the bitumen-water interface at nanoscale resolution using atomic force microscopy. The Canadian Journal of Chemical Engineering. 2007;85:625-634.

[177] Yan L, Englert AH, Masliyah JH, Xu Z. Determination of anisotropic surface characteristics of different phyllosilicates by direct force measurements. Langmuir. 2011;27:12996-13007.

[178] Gao Z, Hu Y, Sun W, Drelich JW. Surface-charge anisotropy of scheelite crystals. Langmuir. 2016;32:6282-6288.

[179] Xie L, Wang J, Shi C, Cui X, Huang J, Zhang H, Liu Q, Liu QX, Zeng H. Mapping the nanoscale heterogeneity of surface hydrophobicity on the sphalerite mineral. The Journal of Physical Chemistry C. 2017;121:5620-5628.

[180] Fritzsche J, Peuker UA. Particle adhesion on highly rough hydrophobic surfaces: The distribution of interaction mechanisms. Colloids and Surfaces A: Physicochemical and Engineering Aspects. 2014;459:166-171.

[181] Rudolph M, Peuker UA. Hydrophobicity of minerals determined by atomic force microscopy - A tool for flotation research. Chemie Ingenieur Technik. 2014;86:865-873.

[182] Rudolph M, Peuker UA. Mapping hydrophobicity combining AFM and Raman spectroscopy. Minerals Engineering. 2014;66-68:181-190.

[183] Dazzi A, Prater CB. AFM-IR: Technology and applications in nanoscale infrared spectroscopy and chemical imaging. Chemical Reviews. 2016; 117:5146-5173.